Frequency combs induced by phase turbulence

Frequency combs induced by phase turbulence

Marco Piccardo[†],[1] Benedikt Schwarz[†],[1,2] Dmitry Kazakov,[1] Maximilian Beiser,[2]
Nikola Opačak,[2] Yongrui Wang,[3] Shantanu Jha,[1,4] Johannes Hillbrand,[1,2]
Michele Tamagnone,[1] Wei Ting Chen,[1] Alexander Y. Zhu,[1]
Lorenzo L. Columbo,[5] Alexey Belyanin,[3] and Federico Capasso[1,*]

([†]These authors contributed equally to this work.)

[1]*Harvard John A. Paulson School of Engineering and Applied Sciences, Harvard University, Cambridge, MA 02138, USA*

[2]*Institute of Solid State Electronics, TU Wien, 1040 Vienna, Austria*

[3]*Department of Physics and Astronomy, Texas A&M University, College Station, TX 77843, USA*

[4]*Physics Department, Yale University, New Haven, CT 06511, USA*

[5]*Dipartimento di Elettronica e Telecomunicazioni, Politecnico di Torino, Corso Duca degli Abruzzi 24, 10129 Torino, Italy*

Turbulence is a ubiquitous phenomenon in nature—it can be found everywhere from smoke rising from an extinct candle to water streams that destabilize and become chaotic. These are hydrodynamic examples [1] of the more general concept of wave instability, where a small disturbance in a wave grows in amplitude due to nonlinear interactions. In photonics, wave instabilities result in modulated light waveforms that, in presence of coherent locking mechanisms, can become periodic. These periodic optical waveforms are known as optical frequency combs [2–4]. In ring microresonator combs [5, 6], an injected monochromatic wave gets destabilized due to the interplay of resonator dispersion and Kerr nonlinearity of the constituent crystal. On the other hand, in ring lasers it is well established that an instability should occur only under extreme pumping conditions [7, 8]. Here we show that despite this notion, ring lasers with ultrafast gain recovery [9, 10] can transit into frequency comb regimes at low pumping levels due to phase turbulence [11]—an instability known in hydrodynamics, superconductors and Bose-Einstein condensates. The instability arises from the phase-amplitude coupling of the laser field provided by the linewidth enhancement [12]. The latter produces the needed interplay of dispersive and nonlinear effects. We formulate the instability condition in the framework of the Ginzburg-Landau formalism [11]. The novel localized structures that we observe share several properties with dissipative Kerr solitons, providing a first step in connecting ring lasers and microresonator frequency combs [13].

Despite decades of studies, the development of optical frequency combs continues at a rapid pace [4, 6, 14]. While historically research on frequency combs started from tabletop optical systems, such as Ti:sapphire modelocked lasers that revolutionized optical metrology [2], the following advances in semiconductor and dielectric material processing led to much more compact frequency comb generators. Technological progress went hand in hand with a burst of new applications, such as spectroscopy and chemical sensing, arbitrary radiofrequency waveform generation, optical communications and quantum information. Within the realm of integrated optics of particular interest are two classes of generators: semiconductor lasers and passive microresonators [6, 15], where in the latter the pump is an external continuous-wave laser and the gain stems from the Kerr nonlinearity. In both cases the device starts from single-frequency operation, corresponding to the first lasing mode or

the external pump. To generate a frequency comb, mechanisms capable of creating modes at different frequencies, coupling them, and locking their phases, need to be present in the cavity. In microresonators, above the parametric instability threshold, the external pump induces the appearance of sidebands. By means of cascaded parametric processes the sidebands grow and proliferate [16]. This coherent nonlinear process gives rise to phase-locked frequency combs. In Fabry-Perot semiconductor lasers multimode operation results from inhomogeneous gain saturation. A standing wave created by the first lasing mode (Fig. 1a) leads to a spatially varying distribution of the gain—a phenomenon known as spatial hole burning (SHB). In a dispersive cavity it leads to proliferation of modes with nonequidistant frequencies, where phase locking can be achieved through the nonlinearity of the gain medium itself [17–20].

SHB is not expected to form in a ring cavity, as the clockwise (CW) and counterclockwise (CCW) modes of a ring resonator are not naturally coupled in absence of a well-defined reflection point that breaks the circular symmetry. We show that semiconductor ring lasers [21–23] can nevertheless undergo a single-mode instability due to a phenomenon known in the realm of Ginzburg-Landau theory as phase turbulence [11] and form frequency combs even in absence of spatial or spectral hole burning. Multimode emission and comb formation occur at a pumping level fractionally higher than the lasing threshold. This is in contrast to the Risken-Nummedal-Graham-Haken instability, that also promotes multimode operation of a ring laser but at a non-practical pumping level of at least nine times above threshold [7, 8].

Ring frequency combs

To study the phenomenon of phase turbulence in lasers we use ring quantum cascade lasers (QCLs) [9]. These are monolithic frequency comb generators that combine nonlinearity and gain [10] and have applications in dual-comb spectroscopy [24], metrology [25] and microwave photonics [26]. QCL frequency combs typically adopt the Fabry-Perot geometry (Fig. 1a) and serve the mid-infrared and the terahertz—strategic regions of the electromagnetic spectrum for chemical sensing. They present the advantages of broad tunability by bandstructure engineering, and high portability, as they are electrically pumped and compact. Several works investigated QCL cavities with circular geometry [9, 27–33] but never studied the generation of self-starting frequency combs. In this work we fabricated ring QCLs in a ridge waveguide geometry (Fig. 1c). They emit in the mid-infrared and operate at room temperature under constant electrical injection (Materials and Methods). A small

fraction of light can escape from the ring cavity due to scattering, allowing us to perform a spectral characterization.

Our finding is that at an injection level only fractionally higher than the lasing threshold (typically 1.1-1.5 J_{th}) the ring lasers undergo a transition to a multimode regime (Fig. 1d) that is characteristically different from those observed in Fabry-Perot QCLs (Fig. 1b). The optical spectrum of the ring has fewer modes and exhibits a bell-shaped envelope. As in Fabry-Perot resonators the modes are separated by the roundtrip frequency of the cavity $f_{rt} = c/(2\pi rn)$, where $n = 3.4$ is the effective refractive index of the waveguide. The coherence of the state is manifested by its narrow beat note, which signifies its frequency comb nature, further confirmed by a coherent beat note detection technique (Supplementary Material). A notable feature of the instability is that as the current in the device is increased, the laser can revert back to single mode operation—a feature not observed in regular Fabry-Perot lasers (Supplementary Material). A multimode instability close to threshold was also reported in a ring dye laser [34] but with different features, namely the suppression of the resonant mode and a parametric gain of two side modes separated by about the Rabi frequency.

Ginzburg-Landau theory

To support the experimental evidence of multimode operation we reexamine the theory of lasers with fast gain media. We show that ring frequency combs can be explained on the basis of a phase instability that affects the single mode solution of the complex Ginzburg-Landau equation (CGLE) [11, 35]. CGLE is a nonlinear differential equation that describes spatially-extended systems of coupled nonlinear oscillators. It appears in many branches of physics, such as superconductivity, Bose-Einstein condensation and quantum field theory. In semiconductor laser theory it can be shown that the field dynamics is described by a CGLE assuming fast gain relaxation [36]. While fast relaxation is not valid for a conventional bipolar semiconductor laser (diode laser) it is a well-known property of QCLs. Here we derive from the master equation of lasers with fast gain media [20] the CGLE for the laser field E:

$$\partial_t E = E + (1 + ic_D)\partial_z^2 E - (1 + ic_{NL})|E|^2 E \tag{1}$$

where t is time and z is the spatial coordinate running along the ring cavity (see the Supplementary Material for the analytical derivation). The only two parameters of the equation are

c_D and c_{NL}, which control the stability of the system and relate to dispersive and nonlinear effects. In the case of QCLs, c_D depends on the group velocity dispersion (GVD), while c_{NL} depends on the Kerr coefficient. Bulk Kerr nonlinearity of a semiconductor crystal is small, but its contribution is compensated by a term of the same order given by the linewidth enhancement factor (LEF) [12, 20]. Despite its different nature from the Kerr nonlinearity, the LEF enters both the c_D and c_{NL} terms, and provides phase-amplitude coupling needed for the phase instability.

In CGLE theory, the parameter space spun by c_D and c_{NL} is divided into different stability regions by the Benjamin-Feir lines [11, 37], which are defined by $1 + c_D c_{NL} = 0$. The inner region confined by the lines has stable, purely single-mode solutions, while the solutions lying in the two outer regions exhibit a so-called phase instability [36], that makes them multimode. We investigate the spectral content of the laser field solutions depending on their location in the CGLE parameter space. In Fig. 2a we show the result of space-time domain simulations of a ring QCL for different points in the (c_D, c_{NL})-parameter space determined by typical laser parameters (Supplementary Material). In these numerical simulations we use the full laser model without approximations [20] and CGLE only guides the choice of laser parameters allowing to probe solutions in various points of the parameter space. The computed optical spectra confirm that in the white stable region only single mode solutions are supported, while in the red instability regions the laser attains a multimode regime despite the absence of SHB, as already suggested by another recent theory of ring QCLs based on effective Maxwell-Bloch equations [38]. The (c_D, c_{NL}) coordinates corresponding to our laser parameters as obtained from the measurement of GVD [39] and LEF [40–42] (Fig. 2c,d) are marked in Fig. 2a showing that the experimentally observed multimode instability is compatible with the phase turbulence mechanism.

Emergence of order from turbulence

Space-time simulations allow to resolve the full temporal evolution of the laser (Fig. 2b and Supplementary Movie). Starting from spontaneous emission, discontinuous changes of the laser field are produced. Amplitude fluctuations of the first lasing mode are coupled to phase fluctuations via the LEF or α-parameter $\alpha = (\partial n'/\partial N)/(\partial n''/\partial N)$, where n' and n'' are the real and imaginary parts of the refractive index, respectively, and N is the carrier density [12]. Physically, fluctuations of n' in the QCL active region lead then to fluctuations in the spacing between the lasing mode and the side modes. The shifts of

the latter with respect to the gain peak eventually lead to multimode lasing, despite the absence of SHB. In CGLE theory one describes the resulting dynamical behaviour shown in Fig. 2b as "phase turbulence". This regime is characterized by the presence of chaotic intensity fluctuations with small amplitude that never reach zero and the absence of phase dislocations [43] (for a detailed discussion of the role of turbulence see the Supplementary Material). After a relatively long time interval ($\sim$400′000 roundtrips) the laser reaches a frequency comb regime, where the intensity becomes periodic, with the waveform repeating itself at every roundtrip. While phase turbulence provides a coupling mechanism among the modes via the LEF, which is alternative to SHB occurring in Fabry-Perot lasers, it is the semiconductor saturation nonlinearity via four-wave mixing that for a sufficiently high intracavity field becomes efficient in compensating dispersion through a self-injection mechanism [10]. Besides the conventional description in terms of LEF and GVD [20], the frequency comb formation can be portrayed from the point of view of Ginzburg-Landau theory as the morphogenesis of a regular spatiotemporal pattern. Here the locking process manifests itself as the interaction of confined intensity structures that shift with respect to each other, eventually conforming into a single stable structure (Fig. 2b).

Role of intracavity defects

In demonstrating that phase turbulence lies at the heart of the multimode instability of ring lasers it is quintessential to distinguish it from another mechanism that normally drives the instability—SHB. Here we show that in a ring cavity that supports SHB, the multimode instability leads to a completely different comb state. SHB arises in a cavity in presence of a well-defined reflection point that couples counterpropagating waves. While in a Fabry-Perot cavity the waves are naturally coupled due to reflections off the cleaved facets, in a ring cavity an analogous reflection point—a defect—has to be intentionally introduced. This is because unintentional defects, which may result from imperfections in fabrication, are insufficient to trigger the SHB instability (Supplementary Material). We embed a defect in a ring laser waveguide by means of focused ion beam lithography (Fig. 3a). A simple yet effective way of controlling the defect reflectivity is to etch a narrow slit across the waveguide to create an air gap in the active region of the laser (Fig. 3b). We choose a slit width of 0.5 μm giving $R \approx 22\%$, which is close to the facet reflectivity of an uncoated Fabry-Perot QCL ($R = 29\%$). The defect-engineered laser generates a frequency comb with a spectrum that is drastically different from that of a ring without an intentional defect (Fig. 3c). It exhibits

an irregular envelope—the result of complex laser mode competition—similar to that of Fabry-Perot devices, where multimode operation is dominated as well by SHB. Presence of optical standing waves enabling SHB is witnessed by the beatnote pattern measured along the cavity with a maximum located, as expected, at the engineered defect (Fig. 3d, Supplementary Material). Space-time simulations of this laser confirm a different dynamics from that of non-engineered rings. The instability shows large intensity fluctuations and a fragmented temporal evolution (Fig. 3e). Locking occurs over a shorter time interval ($\sim$10′000 roundtrips) and results in a nearly flat intensity waveform, as in Fabry-Perot QCL combs [20]. These results show that high reflectivity values, comparable to those of uncoated Fabry-Perot resonators, are needed to mask the effects of phase turbulence in a ring and enable multimode emission due to SHB.

Discussion

Linking the physics of ring lasers to the CGLE suggests a connection with Kerr-driven frequency comb generators. The latter are usually described by the Lugiato-Lefever equation [13] (LLE) with well-known soliton solutions [44–47] derived from the CGLE with coherent forcing in the limit of large values of c_D and c_{NL} parameters. At the same time we showed that the LEF, which intervenes in both Ginzburg-Landau parameters in the case of a ring laser, adds up to contributions of the Kerr nonlinearity and the GVD. The interplay of dispersive and nonlinear effects is essential to produce a self-starting instability, as it is in the case of the modulation instability that lies at the origin of Kerr solitons in microresonators [47].

The link with Kerr combs can be seen not only on the basis of the governing equations but also from the optical spectra. The bell-shaped envelope of QCL ring combs fits well to a sech^2 function (Fig. 1d, Fig. 2a), which is characteristic of dissipative Kerr solitons. The observation of spectral gaps in certain devices (Supplementary Material) is also reminiscent of the variety of Kerr soliton spectra measured for different pump detuning conditions [44, 45]. These observations indicate that necessary, though not sufficient, conditions exist in ring QCLs for the formation of solitonic structures [38]. It is known from Ginzburg-Landau theory that the CGLE admits localized structures as solutions—just like the LLE—such as "modulation amplitude waves" [48]. These appear in the regime of phase turbulence and exhibit weak amplitude modulations on a homogeneous background—features also observed in our numerical simulations of ring QCLs (Fig. 2b) and supported by the experimental character-

ization of the spectral phases of these lasers (Supplementary Material). In the simulations we find that the number of structures in multisolitonic states such as the one reported in Fig. 2b vary stochastically with the laser initial conditions: by only changing the seed of the spontaneous emission noise and repeating the same simulation we obtained a laser state with four structures rather than three (Supplementary Material). This is a clear indication of a multistability phenomenon, which is typical of dissipative solitons in extended systems such as Kerr microcombs.

We also highlight a historical analogy with the progress in the field of passive microresonators: prior theoretical studies by Lugiato and co-workers on transverse patterns in lasers [49, 50], temporally contiguous with the well-known work with Lefever on transverse patterns in passive optical systems [13], derived an equation with a mathematical form very similar to our CGLE, which however describes longitudinal patterns in ring lasers. This is reminiscent of the history of microresonators, in which the LLE anticipated the first experimental demonstration of Kerr combs [51], which also dealt with longitudinal patterns and were later traced back to the LLE.

Besides the several analogies between the two classes of localized structures/combs in Kerr microresonators and ring QCLs that have been highlighted so far, we believe that exist few fundamental differences that would imply different "solitonic" properties (e.g. response to external addressing, mutual interaction), but whose exhaustive study would require a dedicated future work. They mainly rely in the different kind of nonlinearity providing the phase locking between competing modes and the absence of a forcing field in ring QCLs, which might give an advantage to this devices in terms of compactness. In fact while the pumping of passive microresonators requires energy incoming though optical injection, which is responsible for the appearance of a strong central mode in the comb spectrum undesirable in many applications, QCL combs operate without an injected field. In this regard QCLs are more similar to the recently demonstrated laser cavity-soliton microcombs [52]—Kerr microcavities nested in an amplifying fiber loop providing gain—but yet more compact. A ring QCL acting as an electrically-pumped microresonator would hold a significant technological potential, in particular considering the strategic spectral ranges covered by QCLs. Further improvements in this direction should concentrate on the design of efficient light outcouplers—with the precaution of not perturbing the physics of the phase turbulence instability—and on the extension of the comb bandwidth that, differently from the case of Fabry-Perot QCLs, is

not limited by SHB but only by the LEF and GVD.

* capasso@seas.harvard.edu

[1] O. Reynolds, Philosophical Transactions of the Royal Society of London **174**, 935 (1883).

[2] T. W. Hänsch, Rev. Mod. Phys. **78**, 1297 (2006).

[3] T. Udem, R. Holzwarth, and T. W. Hänsch, Nature **416**, 233 (2002).

[4] N. Picqué and T. W. Hänsch, Nature Photonics **13**, 146 (2019).

[5] K. J. Vahala, Nature **424**, 839 (2003).

[6] A. L. Gaeta, M. Lipson, and T. J. Kippenberg, Nature Photonics **13**, 158 (2019).

[7] H. Risken and K. Nummedal, Journal of Applied Physics **39**, 4662 (1968).

[8] R. Graham and H. Haken, Zeitschrift für Physik **213**, 420 (1968).

[9] E. Mujagić, S. Schartner, L. K. Hoffmann, W. Schrenk, M. P. Semtsiv, M. Wienold, W. T. Masselink, and G. Strasser, Applied Physics Letters **93**, 011108 (2008).

[10] A. Hugi, G. Villares, S. Blaser, H. C. Liu, and J. Faist, Nature **492**, 229 (2012).

[11] I. S. Aranson and L. Kramer, Rev. Mod. Phys. **74**, 99 (2002).

[12] C. Henry, IEEE Journal of Quantum Electronics **18**, 259 (1982).

[13] L. A. Lugiato and R. Lefever, Phys. Rev. Lett. **58**, 2209 (1987).

[14] M. Kues, C. Reimer, J. M. Lukens, W. J. Munro, A. M. Weiner, D. J. Moss, and R. Morandotti, Nature Photonics **13**, 170 (2019).

[15] T. J. Kippenberg, R. Holzwarth, and S. A. Diddams, Science **332**, 555 (2011).

[16] T. Herr, K. Hartinger, J. Riemensberger, C. Y. Wang, E. Gavartin, R. Holzwarth, M. L. Gorodetsky, and T. J. Kippenberg, Nature Photonics **6**, 480 (2012).

[17] G. P. Agrawal, Journal of the Optical Society of America B **5**, 147 (1988).

[18] J. Faist, G. Villares, G. Scalari, M. Rosch, C. Bonzon, A. Hugi, and M. Beck, Nanophotonics **5**, 272 (2016).

[19] M. Piccardo, P. Chevalier, T. S. Mansuripur, D. Kazakov, Y. Wang, N. A. Rubin, L. Meadowcroft, A. Belyanin, and F. Capasso, Opt. Express **26**, 9464 (2018).

[20] N. Opačak and B. Schwarz, Phys. Rev. Lett. **123**, 243902 (2019).

[21] N. Matsumoto and K. Kumabe, Japanese Journal of Applied Physics **16**, 1395 (1977).

[22] T. Krauss, P. J. R. Laybourn, and J. Roberts, Electronics Letters **26**, 2095 (1990).

[23] L. Gelens, S. Beri, G. Van der Sande, G. Mezosi, M. Sorel, J. Danckaert, and G. Verschaffelt, Phys. Rev. Lett. **102**, 193904 (2009).

[24] G. Villares, A. Hugi, S. Blaser, and J. Faist, Nat. Commun. **5**, 5192 (2014).

[25] L. Consolino, M. Nafa, F. Cappelli, K. Garrasi, F. P. Mezzapesa, L. Li, A. G. Davies, E. H. Linfield, M. S. Vitiello, P. De Natale, and S. Bartalini, Nature Communications **10**, 2938 (2019).

[26] M. Piccardo, M. Tamagnone, B. Schwarz, P. Chevalier, N. A. Rubin, Y. Wang, C. A. Wang, M. K. Connors, D. McNulty, A. Belyanin, and F. Capasso, Proceedings of the National Academy of Sciences **116**, 9181 (2019).

[27] R. Szedlak, T. Hisch, B. Schwarz, M. Holzbauer, D. MacFarland, T. Zederbauer, H. Detz, A. M. Andrews, W. Schrenk, S. Rotter, and G. Strasser, Scientific Reports **8**, 7998 (2018).

[28] P. Malara, R. Blanchard, T. S. Mansuripur, A. K. Wojcik, A. Belyanin, K. Fujita, T. Edamura, S. Furuta, M. Yamanishi, P. de Natale, and F. Capasso, Applied Physics Letters **102**, 141105 (2013).

[29] A. K. Wojcik, P. Malara, R. Blanchard, T. S. Mansuripur, F. Capasso, and A. Belyanin, Applied Physics Letters **103**, 231102 (2013).

[30] D. G. Revin, M. Hemingway, Y. Wang, J. W. Cockburn, and A. Belyanin, Nature Communications **7**, 11440 (2016).

[31] J. Faist, C. Gmachl, M. Striccoli, C. Sirtori, F. Capasso, D. L. Sivco, and A. Y. Cho, Applied Physics Letters **69**, 2456 (1996).

[32] C. Gmachl, F. Capasso, E. E. Narimanov, J. U. Nöckel, A. D. Stone, J. Faist, D. L. Sivco, and A. Y. Cho, Science **280**, 1556 (1998).

[33] Q. J. Wang, C. Yan, N. Yu, J. Unterhinninghofen, J. Wiersig, C. Pflügl, L. Diehl, T. Edamura, M. Yamanishi, H. Kan, and F. Capasso, Proceedings of the National Academy of Sciences **107**, 22407 (2010).

[34] L. W. Hillman, J. Krasiński, R. W. Boyd, and C. R. Stroud, Phys. Rev. Lett. **52**, 1605 (1984).

[35] K. Staliunas, Phys. Rev. A **48**, 1573 (1993).

[36] L. Gil and G. L. Lippi, Phys. Rev. Lett. **113**, 213902 (2014).

[37] H. Chate, Nonlinearity **7**, 185 (1994).

[38] L. L. Columbo, S. Barbieri, C. Sirtori, and M. Brambilla, Opt. Express **26**, 2829 (2018).

[39] D. Hofstetter and J. Faist, IEEE Photonics Technology Letters **11**, 1372 (1999).

[40] L. Jumpertz, F. Michel, R. Pawlus, W. Elssser, K. Schires, M. Carras, and F. Grillot, AIP Advances **6**, 015212 (2016).

[41] J. von Staden, T. Gensty, W. Elser, G. Giuliani, and C. Mann, Opt. Lett. **31**, 2574 (2006).

[42] N. Kumazaki, Y. Takagi, M. Ishihara, K. Kasahara, A. Sugiyama, N. Akikusa, and T. Edamura, Japanese Journal of Applied Physics **47**, 6320 (2008).

[43] B. Shraiman, A. Pumir, W. van Saarloos, P. Hohenberg, H. Chat, and M. Holen, Physica D: Nonlinear Phenomena **57**, 241 (1992).

[44] T. J. Kippenberg, A. L. Gaeta, M. Lipson, and M. L. Gorodetsky, Science **361** (2018).

[45] T. Herr, V. Brasch, J. D. Jost, C. Y. Wang, N. M. Kondratiev, M. L. Gorodetsky, and T. J. Kippenberg, Nature Photonics **8**, 145 (2014).

[46] D. C. Cole, E. S. Lamb, P. DelHaye, S. A. Diddams, and S. B. Papp, Nature Photonics **11**, 671 (2017).

[47] M. Karpov, M. H. P. Pfeiffer, H. Guo, W. Weng, J. Liu, and T. J. Kippenberg, Nature Physics **15**, 1071 (2019).

[48] L. Brusch, M. G. Zimmermann, M. van Hecke, M. Bär, and A. Torcini, Phys. Rev. Lett. **85**, 86 (2000).

[49] L. A. Lugiato, C. Oldano, and L. M. Narducci, J. Opt. Soc. Am. B **5**, 879 (1988).

[50] W. Kaige, N. B. Abraham, and L. A. Lugiato, Phys. Rev. A **47**, 1263 (1993).

[51] P. Del'Haye, A. Schliesser, O. Arcizet, T. Wilken, R. Holzwarth, and T. J. Kippenberg, Nature **450**, 1214 (2007).

[52] H. Bao, A. Cooper, M. Rowley, L. Di Lauro, J. S. Totero Gongora, S. T. Chu, B. E. Little, G.-L. Oppo, R. Morandotti, D. J. Moss, B. Wetzel, M. Peccianti, and A. Pasquazi, Nature Photonics **13**, 384 (2019).

[53] C. A. Wang, B. Schwarz, D. F. Siriani, L. J. Missaggia, M. K. Connors, T. S. Mansuripur, D. R. Calawa, D. McNulty, M. Nickerson, J. P. Donnelly, K. Creedon, and F. Capasso, IEEE Journal of Selected Topics in Quantum Electronics **23**, 1 (2017).

[54] M. Lončar, B. G. Lee, L. Diehl, M. Belkin, F. Capasso, M. Giovannini, J. Faist, and E. Gini, Optics Express **15**, 4499 (2007).

[55] M. Piccardo, D. Kazakov, N. A. Rubin, P. Chevalier, Y. Wang, F. Xie, K. Lascola, A. Belyanin, and F. Capasso, Optica **5**, 475 (2018).

Materials and Methods

Quantum cascade lasers. The lasers emit around 8 μm and have a structure consisting of GaInAs/AlInAs layers on an InP substrate. The waveguide width is 10 μm and the inner radius r is 500 or 600 μm. The active region consists of AlInAs/GaInAs/InP layers and the band structure design is based on a single-phonon continuum depopulation scheme [53]. The lasers are operated under constant electrical injection with a low-noise current driver (Wavelength Electronics QCL LAB 1500), and their temperature is stabilized at 16°C using a low-thermal-drift temperature controller (Wavelength Electronics TC5). The threshold current density of a symmetric ring was observed to be as low as 1.1 kA/cm^2, while that of the defect-engineered ring was 1.3 kA/cm^2. The increase in threshold current density in the defect-engineered ring is attributed to the losses induced by the defect. For comparison the threshold current density of a Fabry-Perot device fabricated from the same material, with the same waveguide width and cleaved to have approximately the same length of the symmetric ring (L =3.7 mm) was 1.4 kA/cm^2. Only a small amount of light ($\lesssim$ 1 mW) scatters out of the ring waveguide, minimizing the perturbations due to outcoupling on the intrinsic states of the lasers. The laser spectral output is measured using a Fourier transform infrared spectrometer and a sensitive photodetector (HgCdTe detector cooled at 77 K). Beat notes produced during frequency comb operation are electrically extracted from the laser chip using a radiofrequency probe connected to a spectrum analyzer and exhibit a narrow (sub-kHz) linewidth. The symmetry of the optical spectra of ring combs is a further indication of the coherence of these states. The suppression of the central optical mode, which can be observed in certain devices (Supplementary Material), is a signature of a parametric process and reminds of the spectra of frequency-modulated combs. Since the group velocity dispersion (GVD) and linewidth enhancement factor (LEF) characterizations rely on techniques [39–41] for which the output power from a ring would be insufficient, we measure these quantities using Fabry-Perot devices fabricated from the same material and having the same waveguide width of the rings (10 μm). More details on the LEF characterization are given in the Supplementary Material.

Numerical simulations. The theory presented in this work is backed up by numerical simulations that are based on the laser master equation. This was derived in Ref. [20] starting from the full Maxwell-Bloch system of equations. This allows for a considerable increase in implementation efficiency compared to the full Maxwell-Bloch system, while keeping the same fidelity of the model in the case of a fast gain medium, such as QCLs. To furthermore improve the calculation speed,

the code was highly parallelised and implemented in CUDA platform, called from a Python C++ extension interface. The calculations are hence conducted on a graphics processing unit (GPU) within a PC, which allows for extremely short computation times compared to a standard code implementation on a central processing unit (CPU). We used an NVIDIA GeForce GTX 1070 Ti GPU which resulted in a speedup factor of 500 compared to the CPU implementation. As an example, the space-time simulation shown in Fig. 2b, which consists of 600 million time steps, took 27 minutes to run.

Defect engineering. We use focused ion beam (FIB) milling to engineer defects in ring QCLs. FIB is a maskless dry etching technique originally developed for repair of photolithography masks as well as for preparation of samples for transmission electron microscopy. The writing settings for the rectangular pattern are 0.6×10 μm with a depth setting of 1.43 μm. The actual width of the slit cut by FIB (FEI Helios 660) across the ring waveguide is 500 nm. The dwell time is 1 μs and the current is 0.43 nA. The recipe was finely tuned to avoid devastating effects of Ga^+ ions getting implanted in QCL layers, effectively creating a current leakage path of high resistance, that burnt during laser operation [54]. We also had to account for the systematic spatial shifts between the written patterns and the location of the focus of the beam. The reflectivity of the defect is calculated using the frequency domain electromagnetic wave model (*emw* module) of COMSOL. We confirmed the values of defect reflectivity obtained from COMSOL simulations with a calculation using the transfer matrix formalism for a dielectric-air-dielectric interface. The reflectivity peak corresponds to a defect width of approximately quarter wavelength in air (≈ 2 μm) and its value (64%) is dictated by the air-dielectric index contrast. If needed, higher values of reflectivity could be achieved by defining a distributed Bragg reflector (DBR) section in the waveguide using FIB milling.

Radiofrequency gratings. For the measurement of the radiofrequency (or dynamic) gratings we use a coaxial RF probe (Quater A-20338) mounted on an XYZ micrometer positioning stage and placed in contact with the top electrode of the rings. The scanning probe is manually positioned along the perimeter of the ring laser cavity [55]. The signal detected from the probe at every position is amplified with a RF amplifier (CTT ALN 300-8023, bandwidth 18-26.5 GHz, 22 dB gain) and recorded with a spectrum analyzer (Agilent E4448A). The specified 3dB bandwidth of the probe (DC-18 GHz) is smaller than the typical beat note frequency of the ring lasers (23-27 GHz), however the extracted RF signal is still largely sufficient to characterize the beat note

power distribution along the ring cavity.

Acknowledgements

We acknowledge support from the National Science Foundation under Awards No. CCSS-1807323. Any opinions, findings, conclusions or recommendations expressed in this material are those of the authors and do not necessarily reflect the views of the National Science Foundation. This work was performed in part at the Center for Nanoscale Systems (CNS), a member of the National Nanotechnology Coordinated Infrastructure Network (NNCI), which is supported by the National Science Foundation under NSF Award no. 1541959. B.S. was supported by the Austrian Science Fund (FWF) within the project NanoPlas. We gratefully acknowledge C. A. Wang, M. K. Connors and D. McNulty for providing quantum cascade laser material. We thank V. Ginis and F. Grillot for useful discussions, G. Strasser for allowing the device fabrication, P. Chevalier for cleaving the devices, and D. Ham group for lending us microwave amplifiers. We acknowledge enriching discussions with L. A. Lugiato on spatial patterns in lasers and Kerr microcombs.

Author contributions

M.P. initiated the project. B.S. and M.B. fabricated the devices. M.P, B.S., D.K. and S.J. carried out the experiments. M.P. derived the grating model. B.S. and N.O. derived the Ginzburg-Landau theory with suggestions from L.L.C.. B.S., N.O. and Y.W. performed the laser space-time domain simulations. D.K., M.T., W.T.C. and A.Y.Z. performed the defect engineering based on simulations from M.P. and D.K.. M.P. wrote most of the manuscript. M.P., N.O., D.K., S.J. wrote sections of the supplemental. A.B. and F.C. supervised the project. M.P., B.S., D.K., M.B., N.O., Y.W., S.J., L.L.C., A.B. and F.C. contributed to the analysis, discussion and writing of the paper.

Competing interests

The authors declare no competing interests.

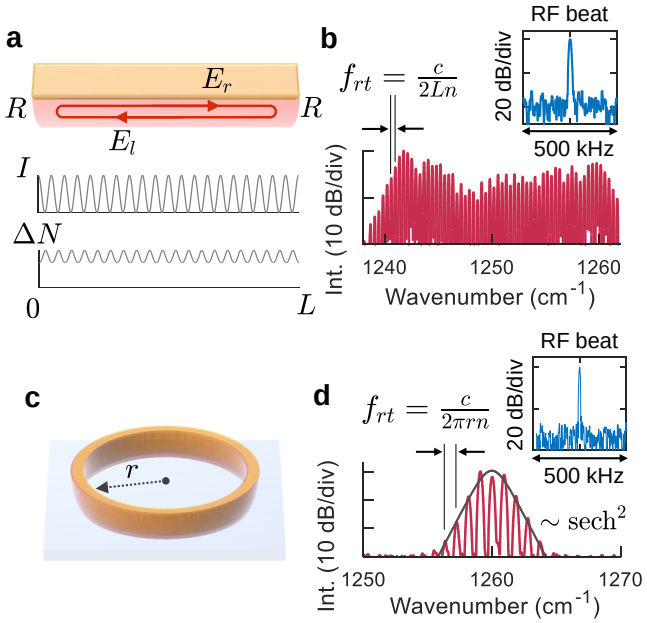

FIG. 1. **Fabry-Perot and ring frequency combs.** **a**, Schematic of a Fabry-Perot cavity with rightward and leftward propagating waves, E_r and E_l, coupled through facets reflectivity R. As a result of counterpropagating waves, optical standing waves of intensity I and a static grating of population inversion ΔN are formed in the cavity of length L. **b**, Experimental optical spectrum of a Fabry-Perot frequency comb generated from a quantum cascade laser ($L = 3.7$ mm). The roundtrip frequency (f_{rt}) defines the comb spacing (11.5 GHz), whose spectrum is shown in the inset. **c**, Schematic of a monolithic semiconductor ring laser of radius r. **d**, Experimental optical spectrum of a ring quantum cascade laser frequency comb ($r = 500$ μm). The envelope of the spectrum is fitted to a sech^2 function for the discussion on solitonic structures. Also shown is the narrow electrical beat note of the laser (central frequency 27.8 GHz). The two lasers are fabricated from the same material. The resolution of the optical spectrum analyzer was 3 GHz in **b** and 6 GHz in **d**, and the resolution bandwidth (RBW) of the radiofrequency spectrum analyzer was 9.1 kHz in **b** and 5.6 kHz in **d**.

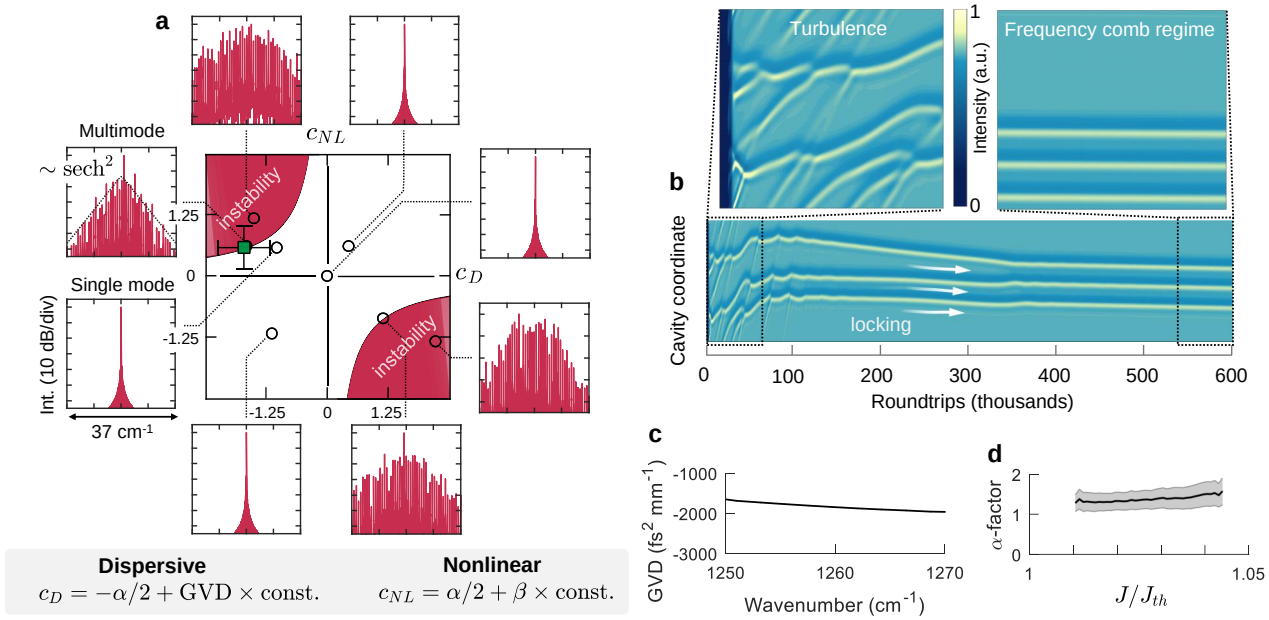

FIG. 2. **Conditions for the phase instability in a monolithic ring laser.** **a** Theoretical spectra obtained by solving the laser master equation are shown for different points in parameter space confirming the behavior expected from Ginzburg-Landau theory. In the simulations spatial hole burning is turned off, thus the obtained multimode regimes are due to the Ginzburg-Landau phase instability. In all plots the x-axis spans 50 longitudinal modes of the ring, the y-axis is intensity (10 dB/div). Also shown is the region corresponding to the experimental devices as obtained from the laser parameters with related uncertainties (square marker). In the simulated spectrum corresponding to this point a sech^2 envelope was fitted to the envelope for the discussion on solitonic structures (dashed line). The formulas shown in the inset are an approximation in the limit of small linewidth enhancement factor (Supplementary Material). **b**, Space-time simulation of the laser dynamics showing the intensity in the ring cavity at every roundtrip. Starting from spontaneous emission (dark stripe in left inset), the laser destabilizes into a turbulent regime and eventually reaches a frequency comb regime. The simulation solves the laser master equation for 600 million time steps (0.05 ms interval). The corresponding point in parameter space is indicated by the square marker in **a**. **c,d**, Measurement of two physical quantities entering in c_D and c_{NL} for a ring quantum cascade laser: GVD is the group velocity dispersion, α is the linewidth enhancement factor (β, the Kerr nonlinearity, is small in QCLs). In **d**, the experimental values are shown as a function of current density normalized to the lasing threshold.

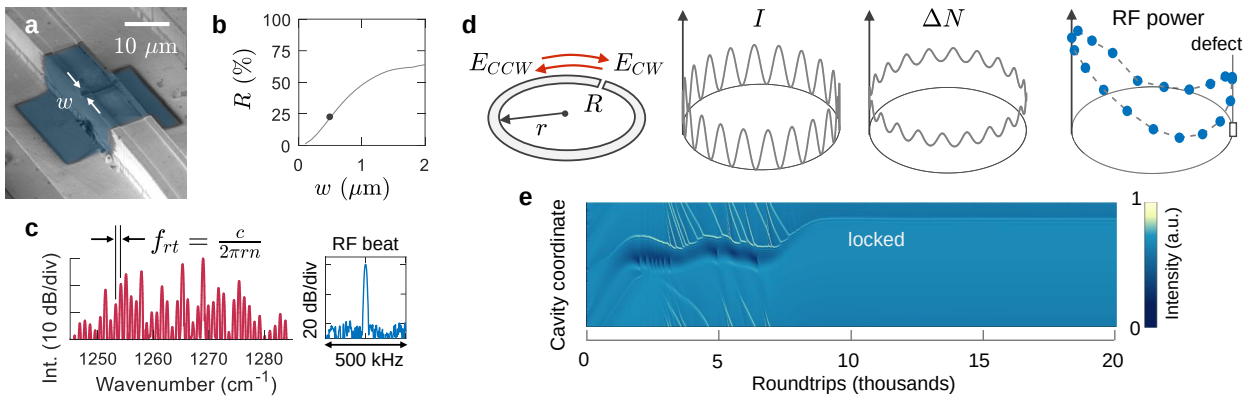

FIG. 3. **Defect-engineered ring frequency comb.** **a**, Scanning electron microscope image of the defect-engineered ring laser showing the aperture in the metal (blue region in false color) with a 0.5 μm wide slit fabricated by focused ion beam lithography. **b**, Reflectivity induced by the slit as a function of its width as calculated from numerical wave simulations. The reflectivity of the studied device is $R \approx 22\%$ (dot). **c**, Experimental optical spectrum of a defect-engineered ring quantum cascade laser ($r = 500$ μm) fabricated from the same material of the other devices studied in this work. Also shown is the microwave beat note extracted from the laser (central frequency 27.8 GHz, RBW 9.1 kHz). **d**, Schematic of the ring laser embedding an engineered defect of reflectivity R. The defect induces clockwise and counterclockwise waves, E_{CW} and E_{CCW}, resulting in an optical standing wave I and a static population grating ΔN. The right panel shows the experimental beat note power pattern (RF power) measured along the perimeter of the ring at the roundtrip frequency indicating a bidirectional regime. **e**, Space-time simulation of a ring laser with a defect ($R = 25\%$).